Mechanical Systems and Signal Processing 140 (2020) 106650

Contents lists available at ScienceDirect

Mechanical Systems and Signal Processing

journal homepage: www.elsevier.com/locate/ymssp

A local specific stiffness identification method based on a multi-scale "weak" formulation

Chao Zhang [a], Hongli Ji [a,*], Jinhao Qiu [a,*], Li Cheng [b], Weixing Yao [a], Yipeng Wu [a]

[a] State Key Laboratory of Mechanics and Control of Mechanical Structures, Nanjing University of Aeronautics and Astronautics, Nanjing, China
[b] Department of Mechanical Engineering, Hong Kong Polytechnic University, Hong Kong, China

ARTICLE INFO

Article history:
Received 25 May 2019
Received in revised form 22 December 2019
Accepted 13 January 2020

Keywords:
Mechanical property
Noise immunity
Structural vibration
Nondestructive testing

ABSTRACT

This paper presents a novel local specific stiffness identification method based on a multi-scale "weak" formulation. Based on the local equation of motion, the specific stiffness of a structure can be extracted from its measured vibration displacement, which can further be used as an indicator of damage occurrence inside the structure. However, the estimation of the high order derivative of the measured displacement via a finite difference scheme is prone to the measurement noise. To tackle this problem, a weight function is utilized as a scanning window, which transforms a "point-by-point" identification strategy to a "region-by-region" paradigm. Through a proper parameter setting of the weight function, the final mathematical expression of the local specific stiffness allows avoiding the direct calculation of the high order derivative, thus improving the identification accuracy under noisy measurement conditions. As a proof-of-concept example, an aluminum cantilever beam is investigated for validating the proposed method. The influences of key parameters, such as measurement interval, scale factor and derivative order of the measured vibration displacement, are investigated. The effectiveness of the proposed method is demonstrated numerically and validated experimentally using a step-shaped beam.

© 2020 Published by Elsevier Ltd.

1. Introduction

To ensure the structural safety and reliability, effective damage detection methods are highly essential. In particular, vibration based damage detection methods have been widely investigated during the recent decades [1]. Relying on the examination of different vibration parameters such as mode shapes [2,3], natural frequencies [4], transfer matrices [5], electro-mechanical impedance [6] or modal curvature *etc.* [7], various types of damage indices have been developed to detect the local structural damage. Along with these methods is the possible deployment of a variety of measurement techniques using Laser Doppler Vibrometer (LDV) [8,9], piezoelectric sensors [10,11] and strain gauges [12,13] *etc.*. As one of the latest developments, "Pseudo-Excitation" (PE) method provides a damage detection framework by evaluating the damage-induced perturbation to the local dynamics of the structure [14,15], which can also be regarded as a local force identification problem in principle [16,17]. Compared with other vibration based damage detection methods, PE method exhibits multiple advantages, mainly in its non-requirement of prior knowledge on the overall structural vibration models, boundary conditions or baseline signals. Furthermore, owing to its local inspection nature, it can be applied to complex structures through examining the corresponding local dynamics of structure component-by-component [18–20].

* Corresponding authors.
E-mail addresses: jihongli@nuaa.edu.cn (H. Ji), qiu@nuaa.edu.cn (J. Qiu).

https://doi.org/10.1016/j.ymssp.2020.106650
0888-3270/© 2020 Published by Elsevier Ltd.

However, the original version of the PE method can only detect the damage location where sudden change occurs in the damage index (DI) curve. Considering that the DI is a complex function of the structural damage, PE method can hardly inform on the damage severity, even though DI quantitatively identifies the deviation from the local equation of motion of the healthy structure. To overcome this drawback, one possible way is the determination of the mechanical properties of the structures, which is closely related with the structural damage, for instance, stiffness [21]. Especially for composite structures, changes in stiffness can be used to quantitatively assess the degradation in mechanical property induced by factors such as fatigue damage accumulation [22], for further achieving the prediction of the structural residual life [23]. Obviously, the material stiffness can usually be measured through the standard tensile test, but the main drawback is that it is destructive which only gives the overall structural stiffness rather than the local property. To overcome these problems, various inverse approaches based on structural dynamic responses, such as wave velocity [24,25] and natural frequency [26,27], have been developed to identify the mechanical properties. Different from the above identification methods, which are usually based on minimizing the difference between the measured dynamic behavior and a pre-established model, a Corrected Force Analysis Technique (CFAT) based material characterization has been developed. Material properties in areas where no external loads are applied can be identified [28]. Furthermore, a broadband identification method for an orthotropic composite plate has been established by evaluating the local equation of motion [29]. Inheriting the features of the original PE method, this method does not need the construction of structural vibration model and the complex iterative process. However, high-order spatial derivative terms of the vibration displacement are still involved. For their calculation, the implementation of the finite difference scheme makes the identification results venerable to the measurement noise.

In recognition of these problems, a local specific stiffness identification method using a spatial multi-scale "weak" formulation is developed in this paper. Different from evaluating the local equation of motion at a given point, a flexible weight function, served as a scanning window, is introduced, allowing converting the identification philosophy from "point-by-point" to "region-by-region". Taking a beam structure as benchmark, the "weak" formulation-based local specific stiffness formula is derived to eliminate the high-order spatial derivative of the displacement, whilst providing an improved robustness against the measurement noise.

The outline of this paper is as follows: Section 2 introduces the basic principle of the local specific stiffness identification method. Influences of the key parameters on the noise immunity capability and the detection accuracy, such as the selection of the measurement interval, the scale factor and the derivative order of the measured vibration displacement are discussed in Section 3. Numerical simulation and experimental validation using a step-shaped beam with a thickness variation are then carried out in Sections 4 and 5 to demonstrate the effectiveness of the proposed method. Finally, conclusions are drawn in Section 6.

2. Identification method based on a multi-scale "weak" formulation

The dynamic response at any given point on a structural component should satisfy a certain equation of motion. This can be mathematically expressed for every given point inside the structure, which is referred to as "strong" formulation. Taking a beam-like structure with homogeneous material properties under a flexural harmonic excitation as an example, the steady vibration displacement $w(x)$ is governed by

$$\tilde{E} I \frac{\mathrm{d}^4 w(x)}{\mathrm{d}x^4} - \rho S \omega^2 w(x) = f(x) \tag{1}$$

where $\tilde{E} = E(1 + \mathrm{j}\eta_E)$ is the complex Young's modulus. E, η_E and j are the Young's modulus, the loss factor and the unit imaginary number. I, ρ and S are the cross-sectional moment of inertia, density of material and cross sectional area of the beam element, respectively. ω is the angular frequency of the excitation and $f(x)$ represents the distributed external force over the beam element, which equals to zero for the beam segment with free-surface under inspection. Since light damping has little effect on the vibration at off-resonant frequencies, only the real part of $\tilde{E}$ is taken into consideration when the excitation frequency is away from any natural frequencies of the whole structure [30].

For a structure with known geometrical parameters, the specific stiffness of the material κ ($\kappa = E/\rho$) can, in principle, be identified by measuring the steady vibration displacement $w(x)$ at a given frequency. The basic idea is to evaluate a κ value which warrants a zero $f(x)$ value within the beam region without any surface loading, irrespective of the boundary condition of the entire structure. Thus, the estimated specific stiffness κ should be the solution of the following "strong" formulation expression

$$f(x)/\rho = \kappa I w^{(4)}(x) - S\omega^2 w(x) = 0 \tag{2}$$

and

$$\kappa = \frac{S\omega^2 w(x)}{I w^{(4)}(x)} \tag{3}$$

where the superscript (4) represents the fourth order derivative. For the implementation of Eq. (3), $w^{(4)}(x)$ can be obtained through finite difference approximation, written as

$$w_i^{(4)} = \frac{1}{d^4}[\ 1 \quad -4 \quad 6 \quad -4 \quad 1\ ][\ w_{i-2} \quad w_{i-1} \quad w_i \quad w_{i+1} \quad w_{i+2}\ ]^T \tag{4}$$

in which the subscript i denotes the i-th measurement point and d is the interval between the adjacent measurement points.

As a commonly used method to calculate the high order derivative, the finite difference approach is inherently tied with the conflicting feature between the truncation error and the noise contamination. Mathematically, the smaller interval d is, the more accurate the finite difference result will be, alongside an increasing noise contamination. Furthermore, it should be mentioned that a corrected finite difference scheme can be used to reduce the bias error when large measurement interval or high frequency excitation is implemented [31].

To tackle this problem, a multi-scale "weak" formulation-based local specific stiffness identification is proposed by examining the vibration displacement in a local region. Considering that the specific stiffness is a constant within the region $[x - \tau, x + \tau]$, the "weak" formulation retrofitted from Eq. (2) can be written in an inner product form, as

$$\int_{-\tau}^{+\tau} \left[\widetilde{\kappa} I w^{(4)}(x+\xi) - S\omega^2 w(x+\xi)\right]\eta(\xi)\mathrm{d}\xi = 0 \tag{5}$$

where ξ is an integral variable, τ is the scale factor and $\eta(x)$ is the weight function which can, in principle, take arbitrary forms. The estimated specific stiffness $\widetilde{\kappa}$ using the "weak" formulation can be obtained by

$$\widetilde{\kappa} = \frac{\int_{-\tau}^{+\tau} S\omega^2 w(x+\xi)\eta(\xi)\mathrm{d}\xi}{\int_{-\tau}^{+\tau} I w^{(4)}(x+\xi)\eta(\xi)\mathrm{d}\xi} \tag{6}$$

Certainly, the specific interest in the local points within the scanning region can be fulfilled by an appropriate selection of $\eta(x)$, with which the local (at a certain point) and overall (within the scanning region) characteristics of the specific stiffness can be balanced.

According to Eq. (6), the high order derivative of the vibration displacement still remains. To take a further step, $\widetilde{\kappa}$ can be extended to a series of variants through integration by part. Especially, when the selection of $\eta(x)$ satisfies the following conditions, as

$$\eta^{(i)}(-\tau) = \eta^{(i)}(+\tau) = 0 \ (i = 0, 1, 2, 3) \tag{7}$$

with $\eta^{(0)}$ denoting $\eta(x)$. The finial form of $\widetilde{\kappa}$ can be written as

$$\widetilde{\kappa} = \frac{\int_{-\tau}^{+\tau} S\omega^2 w(x+\xi)\eta(\xi)\mathrm{d}\xi}{\int_{-\tau}^{+\tau} I w(x+\xi)\eta^{(4)}(\xi)\mathrm{d}\xi} \tag{8}$$

in which the high order derivative is transferred to $\eta(x)$. Therefore, the unwanted derivative operation to get $w^{(4)}(x)$ can thus be avoided.

Furthermore, if the specific stiffness within the inspected local region is a constant, the following variant of the "strong" formulation in Eq. (2) can be obtained, as

$$\kappa I w^{(4+i)}(x) - S\omega^2 w^{(i)}(x) = 0 \ (i = 1, 2, 3\ldots) \tag{9}$$

According to the previous analysis, it is not difficult to find that the "weak" formulation-based specific stiffness $\widetilde{\kappa}$ can be extended to a more general form as

$$\widetilde{\kappa} = \frac{\int_{-\tau}^{+\tau} S\omega^2 w^{(i)}(x+\xi)\eta(\xi)\mathrm{d}\xi}{\int_{-\tau}^{+\tau} I w^{(i)}(x+\xi)\eta^{(4)}(\xi)\mathrm{d}\xi} \tag{10}$$

Thus, an enhanced multi-scale "weak" formulation involving different derivative orders of displacement, $w^{(i)}(x)$, can be obtained as

$$\widetilde{\kappa} = \frac{\sum_{i=0}^{n} \left|\int_{-\tau}^{+\tau} a_i S\omega^2 w^{(i)}(x+\xi)\eta(\xi)\mathrm{d}\xi\right|}{\sum_{i=0}^{n} \left|\int_{-\tau}^{+\tau} a_i I w^{(i)}(x+\xi)\eta^{(4)}(\xi)\mathrm{d}\xi\right|} \tag{11}$$

where a_i is the normalized coefficients of the "weak" formulation corresponding to the i-th derivative of displacement.

Different from the "strong" formulation in Eq. (3), $\widetilde{\kappa}$ can be seen as an indicator to the local specific stiffness within a scanning window. By so doing, the strict prerequisite of satisfying the local equation of motion "point-by-point" is shifted to a different "region-by-region" paradigm. In that sense, the measurement noise can be partly suppressed from "strong" to "weak" modality [15]. Furthermore, it can be seen that the direct benefit of the weak formulation, Eqs. (8) and (11), is to calculate the high order derivative of the weight function, instead of the vibration displacement itself. As a result, the finite difference calculation can be completely or partly avoided to enhance the noise immunity of the identification. It is important to note that the identified $\widetilde{\kappa}$ is a function of x according to the above derivation. Despite the assumption that

the material parameters (E and ρ) are constants in the space domain, the proposed method provides the possibility to assess different material properties inside a local area which can be demonstrated in the following sections.

3. Parameter selections

To further illustrate the identification method discussed in the preceding section, a homogeneous and isotropic cantilever beam is first investigated using finite element simulations. Although the finite element model may not perfectly simulate the structure in the reality, the modelling error can be ignored when the vibration displacement is only used for the comparison between "strong" and "weak" formulations. As shown in Fig. 1, the beam structure is made of aluminum with a specific stiffness κ of 2.6×10^7 m^2/s^2 (Young's modulus E = 70 GPa, density ρ = 2700 kg/m^3). The beam is 650 mm long and 5 mm thick. A harmonic point excitation is applied at the right end of the beam, referenced to the coordinate system shown in Fig. 1. A vibration model is created using the commercial finite element code ABAQUS and the size of the linear beam element with

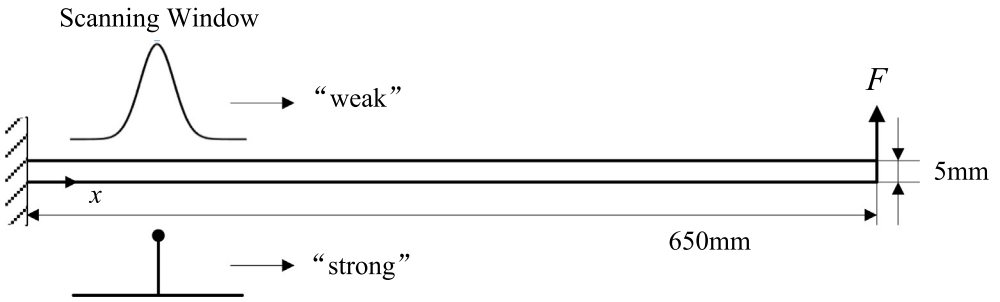

Fig. 1. A cantilever beam for proof-of-concept validation.

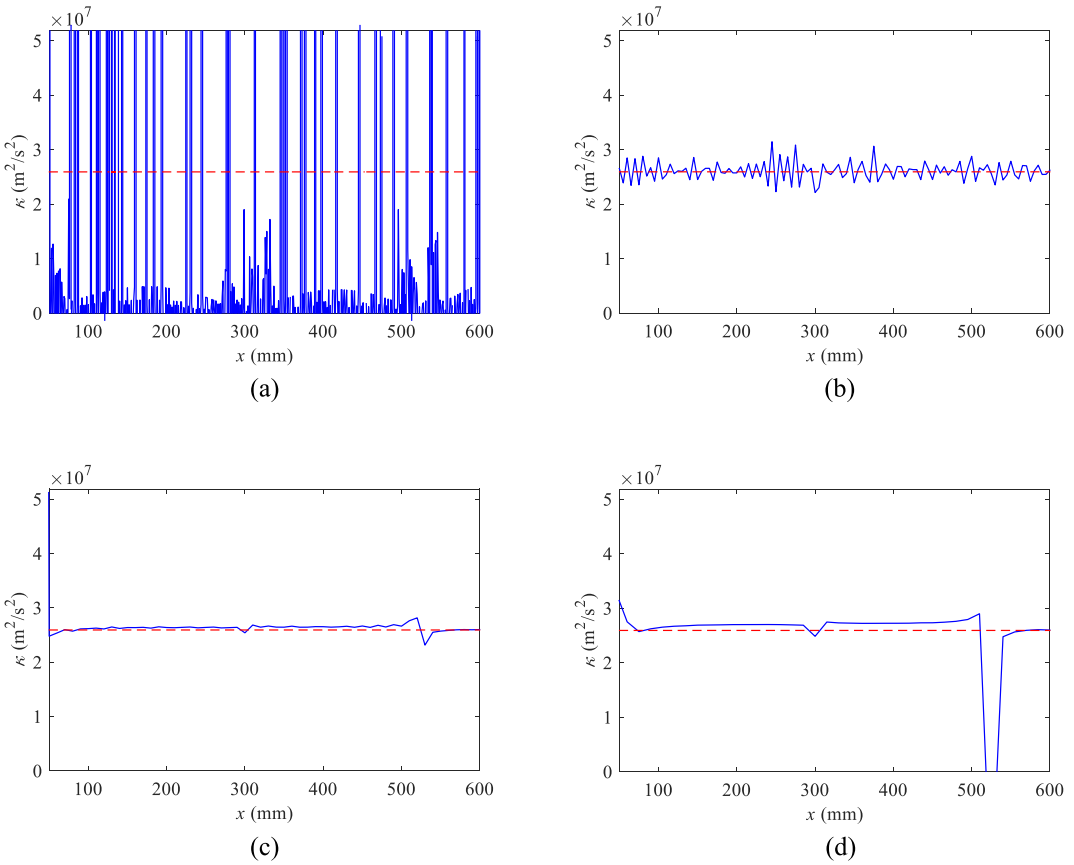

Fig. 2. "Strong" formulation-based identification results using different measurement intervals d: (a) 1 mm, (b) 5 mm, (c) 10 mm and (d) 15 mm.

cubic formulation is set to 1 mm. The structural vibration displacement is obtained at 200 Hz, which is away from any natural frequencies of the structure.

3.1. "Strong" formulation-based method

For comparison, Eq. (3) based on the "strong" formulation is firstly applied to identify the local specific stiffness of the beam. Considering that the high order derivative calculation $w^{(4)}(x)$ is sensitive to the spatial measurement interval d, the identification results with different d, ranging from 1 to 15 mm, are shown in Fig. 2 by using the same vibration displacement data. The constructed κ curves along the beam span show that the expected results are in accord with the actual situation that can be obtained through the adjustment of the measurement interval. When d equals to 1 mm that is the length of the finite element, the error of finite element method is magnified via the finite difference calculation as Eq. (4). Therefore, Fig. 2 (a) is unable to deliver the acceptable identification. As d increases, the identified κ trends approach to the nominal aluminum property in agreement with the previous discussions. It should be mentioned that obvious errors appear at x = 300 mm and x = 525 mm, as shown in Fig. 2(d). According to Fig. 3, both the displacement and its 4th order derivative are close to zero at these points, so that the denominator of Eq. (3) approaches to zero and the identified κ becomes unstable and even singular.

To quantify the detection results, a relative error e of identified κ is defined as

$$e = \frac{1}{N}\sum_{i\in\Omega}\frac{|\kappa_i - \kappa^*|}{\kappa^*} \tag{12}$$

where N is the number of the measurement points within the inspection region Ω and κ^* is the actual value of the specific stiffness. The relative errors based on the "strong" formulation with different measurement intervals are shown in Fig. 4. Considering that the upper and the lower bounds of the identified κ are set to 0 and $2\kappa^*$ respectively, the maximum relative error can reach but capped to 1. The average relative error e gets to a minimum value when the measurement interval is 8 mm and keeps a low level within a wide range. Although it may not theoretically feasible to determine the optimal measurement interval for a given scenario, a balance between the truncation error and the noise disturbance can still be struck through examining the variation pattern of e: typically decreasing at first before reaching a slight increasing trend. Meanwhile, the spatial resolution of the identification decreases as the measurement interval increases.

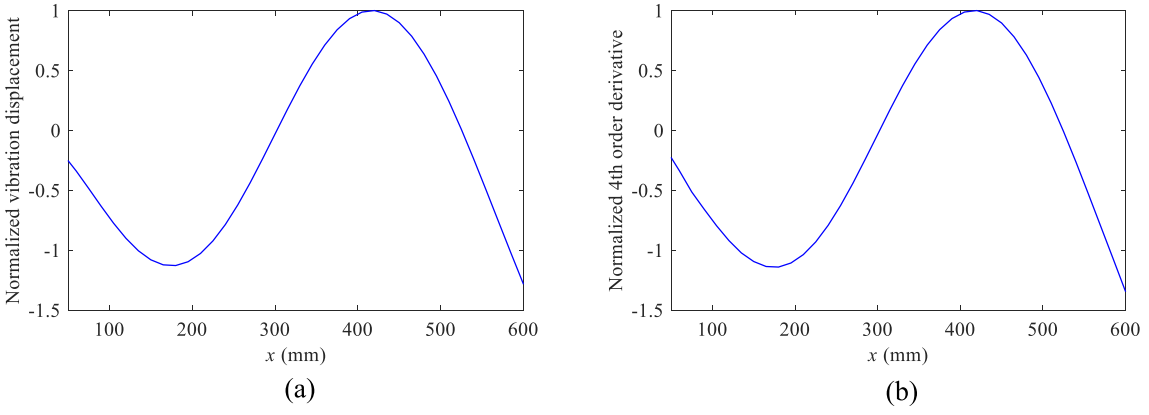

Fig. 3. FE simulated normalized vibration responses of the aluminum beam: (a) vibration displacement and (b) its fourth order derivative.

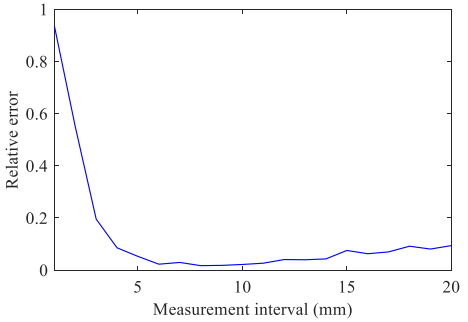

Fig. 4. Relative error of "strong" formulation-based identification results using different measurement intervals.

To quantitatively examine the noise immunity capability of the proposed method, a white Gaussian noise with a standard deviation of 1‰ in the magnitude of $w(x)$ is added to the calculated vibration displacement. In other words, the signal-to-noise ratio (*SNR*) of noisy vibration displacement is 60 dB. Using the same four different measurement intervals, the "strong" formulation-based identification results are shown in Fig. 5. Compared with the results in the absence of the measurement noise in Fig. 2, the identified κ using the noisy displacement is obviously quite different from the actual value with d varying from 1 to 15 mm. The noise effect, magnified in the high order derivative calculation, leads to a large fluctuation of κ, suggesting the low noise robustness of the "strong" formulation. Although the relative error curve in Fig. 6 shows a downward

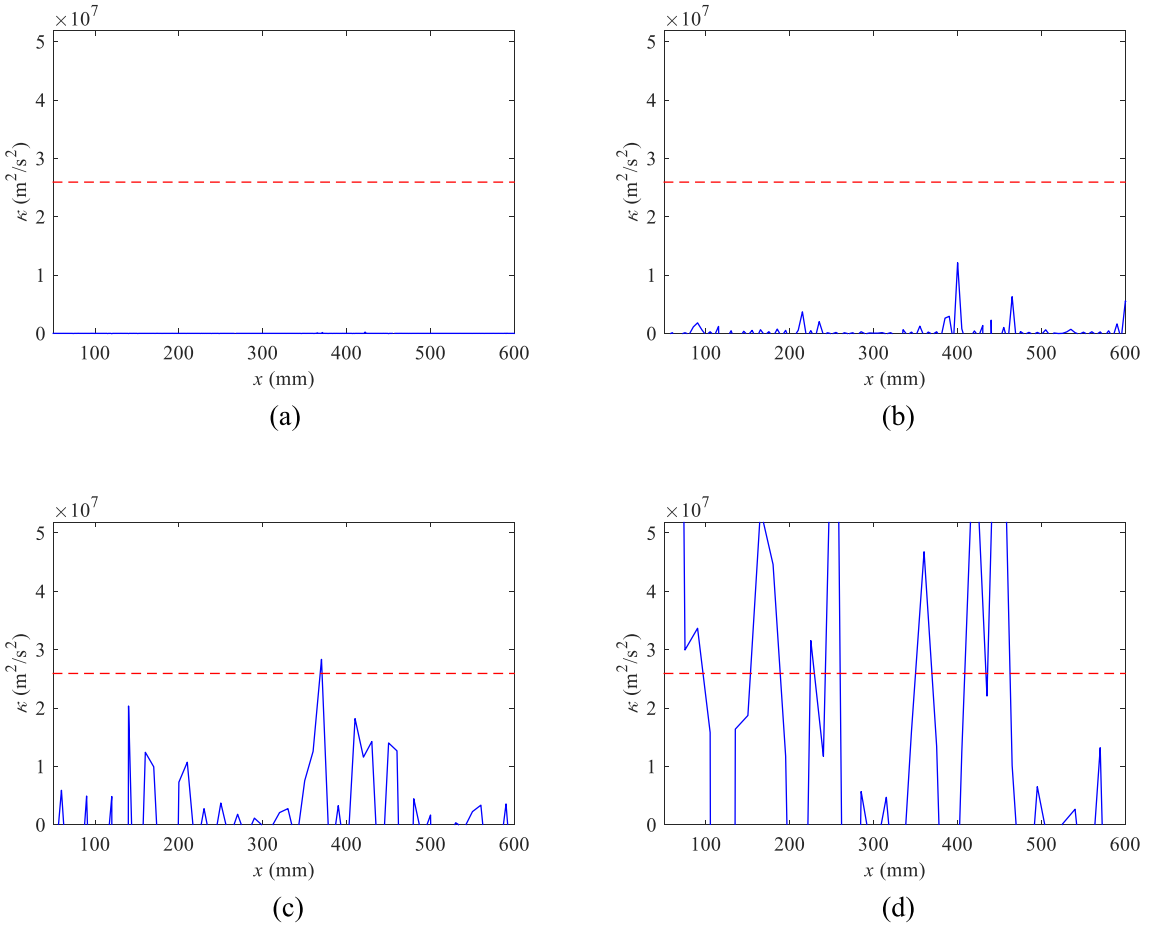

Fig. 5. "Strong" formulation-based identification results using different measurement intervals d with the noisy displacement: (a) 1 mm, (b) 5 mm, (c) 10 mm and (d) 15 mm.

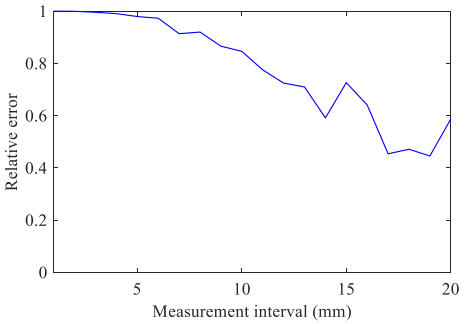

Fig. 6. Relative error of "strong" formulation-based identification results using different measurement intervals with the noisy displacement.

trend when the measurement interval increases, the resulting relative error, typically more than 50%, is unacceptable by any standards.

3.2. "Weak" formulation-based method

The selection of the weight function $\eta(x)$ determines the quality of the "weak" formulation-based local specific stiffness identification. In order to capitalize on the windowing feature of the "weak" formulation and better highlight the local characteristics of the structure while satisfying the boundary conditions in Eq. (7), a power-of-cosine function is utilized as $\eta(x)$, defined by

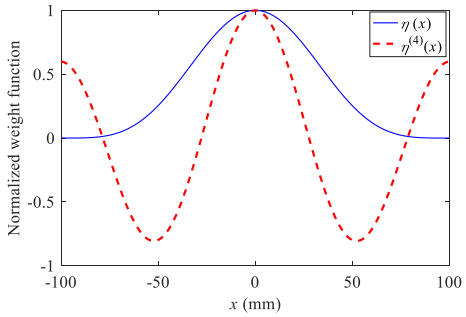

Fig. 7. Curves of the normalized weight function $\eta(x)$ and $\eta^{(4)}(x)$.

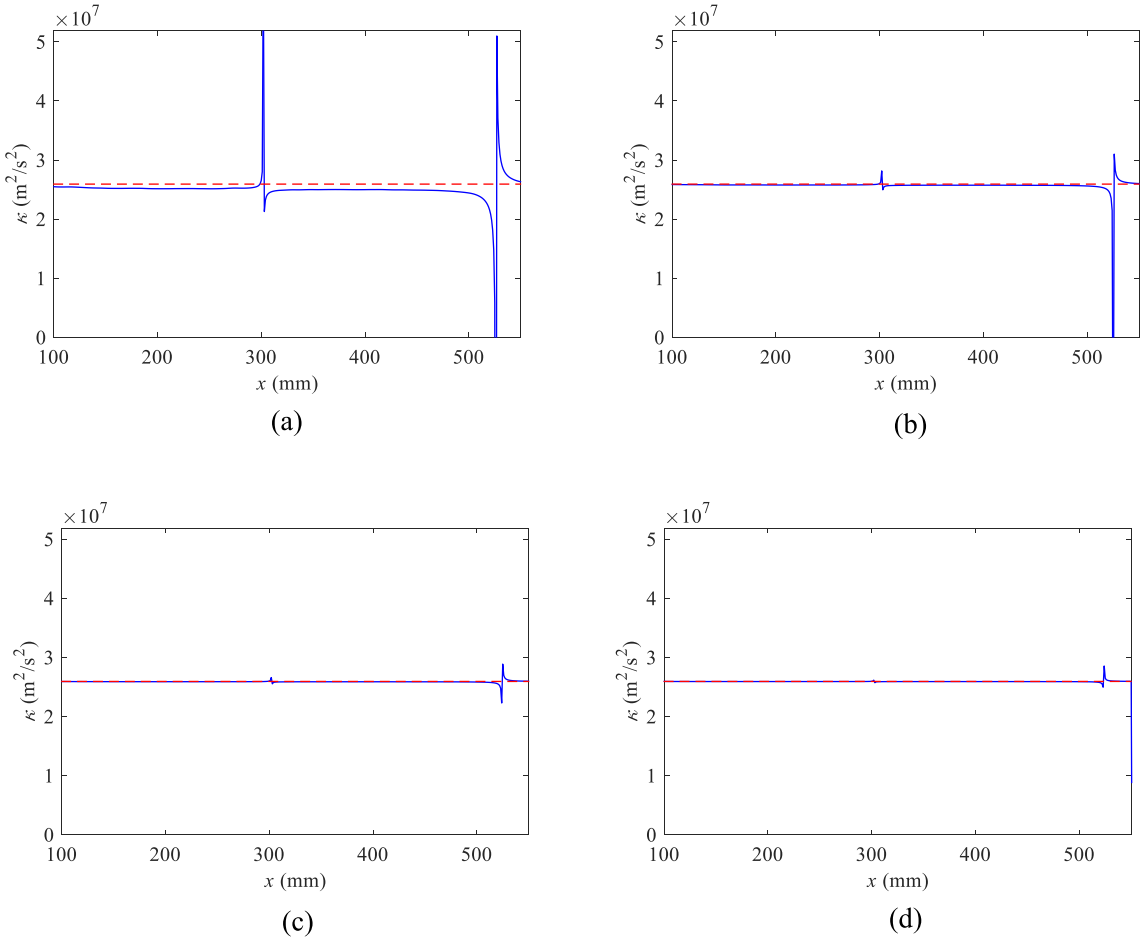

Fig. 8. "Weak" formulation-based identification results using different scale factors τ: (a) τ = 40 mm, (b) τ = 60 mm, (c) τ = 80 mm and (d) τ = 100 mm.

$$\eta(x) = \cos^4\left(\frac{\pi x}{2\tau}\right) \tag{13}$$

where τ is the scale factor that controls the length and the shape of the weight function. The fourth order derivative of the power-of-cosine function can be written as

$$\eta^{(4)}(x) = \frac{3\pi^4}{2\tau^4}\sin^4\left(\frac{\pi x}{2\tau}\right) - \frac{12\pi^4}{\tau^4}\cos^2\left(\frac{\pi x}{2\tau}\right)\sin^2\left(\frac{\pi x}{2\tau}\right) + \frac{5\pi^4}{2\tau^4}\cos^4\left(\frac{\pi x}{2\tau}\right) \tag{14}$$

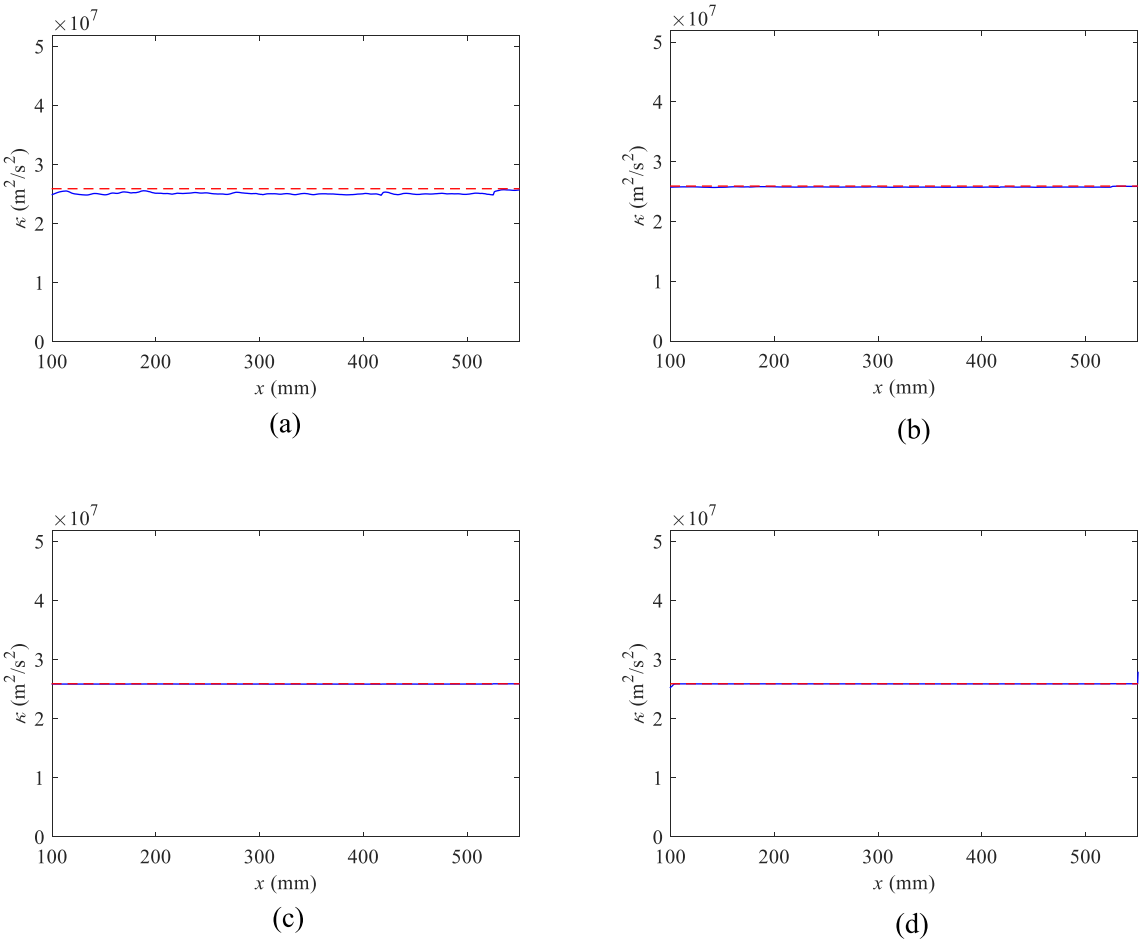

Fig. 9. Enhanced "weak" formulation-based identification results using different scale factors τ: (a) τ = 40 mm, (b) τ = 60 mm, (c) τ = 80 mm and (d) τ = 100 mm.

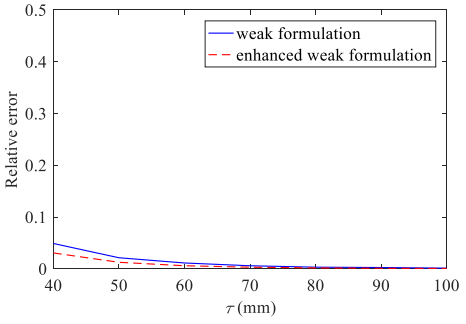

Fig. 10. Relative error using different values of τ in the "weak" formulation-based methods.

As shown by the solid line in Fig. 7, the prominent advantage of the power-of-cosine function is that the weighting is mainly focused on the central region and spreads to zero at the boundaries of the window. This property also holds for the 1st to 3rd order derivatives of the weight function. Therefore, the "weak" formulation-based method using the power-of-cosine function acts like a smooth regional scanner, rather than a point inspector as shown in Fig. 1. The spatial resolution of the "weak" formulation-based method can be regulated by the scale factor τ. It should be mentioned that other functions can also be used as long as the boundary conditions in Eq. (7) are satisfied, such as a polynomial function ($\eta(x) = (1 - (x/\tau)^2)^4$).

The vibration displacement with the measurement interval d = 1 mm is then processed with the "weak" formulation-based method as Eq. (8). The constructed $\widetilde{\kappa}$ with different τ, 40 mm, 60 mm, 80 mm and 100 mm, respectively, are shown in Fig. 8. It is obvious that the specific stiffness can be identified effectively by the $\widetilde{\kappa}$ curves in the absence of the noise interference. For the most of regions in Fig. 8, $\widetilde{\kappa}$ equals to the nominal aluminum property values marked by the dotted line. Same as the "strong" formulation-based method, obvious errors appear at x = 300 mm and 525 mm, due to the fact that both the displacement and its 4th order derivative are close to zero at these points.

The enhanced version of the multi-scale "weak" formulation-based method is then used to solve this problem. In order to avoid the high order finite difference calculation, n is set to 1 in Eq. (11), *i.e.* only $w(x)$ and $w^{(1)}(x)$ are used in the calculation process. With the normalized coefficients a_i set to the reciprocal of the amplitude of $w^{(i)}(x)$, the identified results with different scale factors are shown in Fig. 9. The relative error plotted in Fig. 10 shows that the enhanced multi-scale "weak" formulation-based method further reduces the relative error. Meanwhile, the obvious errors around the vibration nodes shown in Fig. 9 disappear. Because of the different node locations of $w(x)$ and $w^{(1)}(x)$, Eq. (11) avoids the problem of zero denominator in Eqs. (3) and (8).

Upon imposing the same noise as used in the previous discussion, the identified $\widetilde{\kappa}$ based on the "weak" formulation using different τ are shown in Fig. 11. Given a smaller τ (as shown in Fig. 11(a)), the noise effect can be observed clearly, which

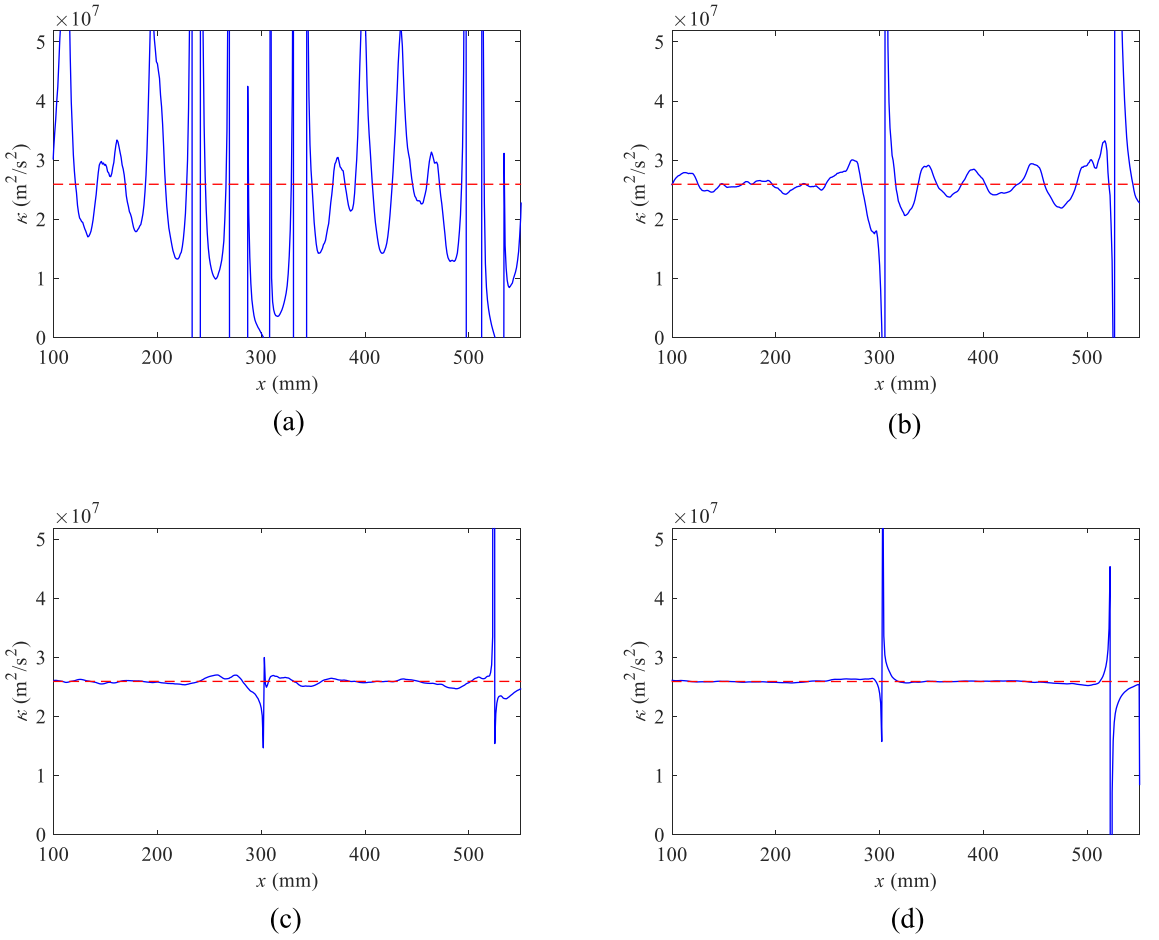

Fig. 11. "Weak" formulation-based identification results using different scale factors with the noisy displacement: (a) τ = 40 mm, (b) τ = 60 mm, (c) τ = 80 mm and (d) τ = 100 mm.

eventually can mask the actual value of the specific stiffness. It implies that the noise robustness of the "weak" formulation-based method is limited when the scale factor τ is small. With a larger τ, the noise induced oscillation in the $\widetilde{\kappa}$ curve decreases because of the enhanced averaging effect of the measurement noise through the extension of the power-of-cosine function. A satisfactory result can be obtained when $\tau \geq 80$ mm. Similar phenomena can be observed when using the enhanced "weak" formulation-based method as illustrated in Fig. 12. A detailed evaluation of the identified results is shown in Fig. 13. The relative error of the enhanced "weak" formulation-based method using both $w(x)$ and $w^{(1)}(x)$ increases

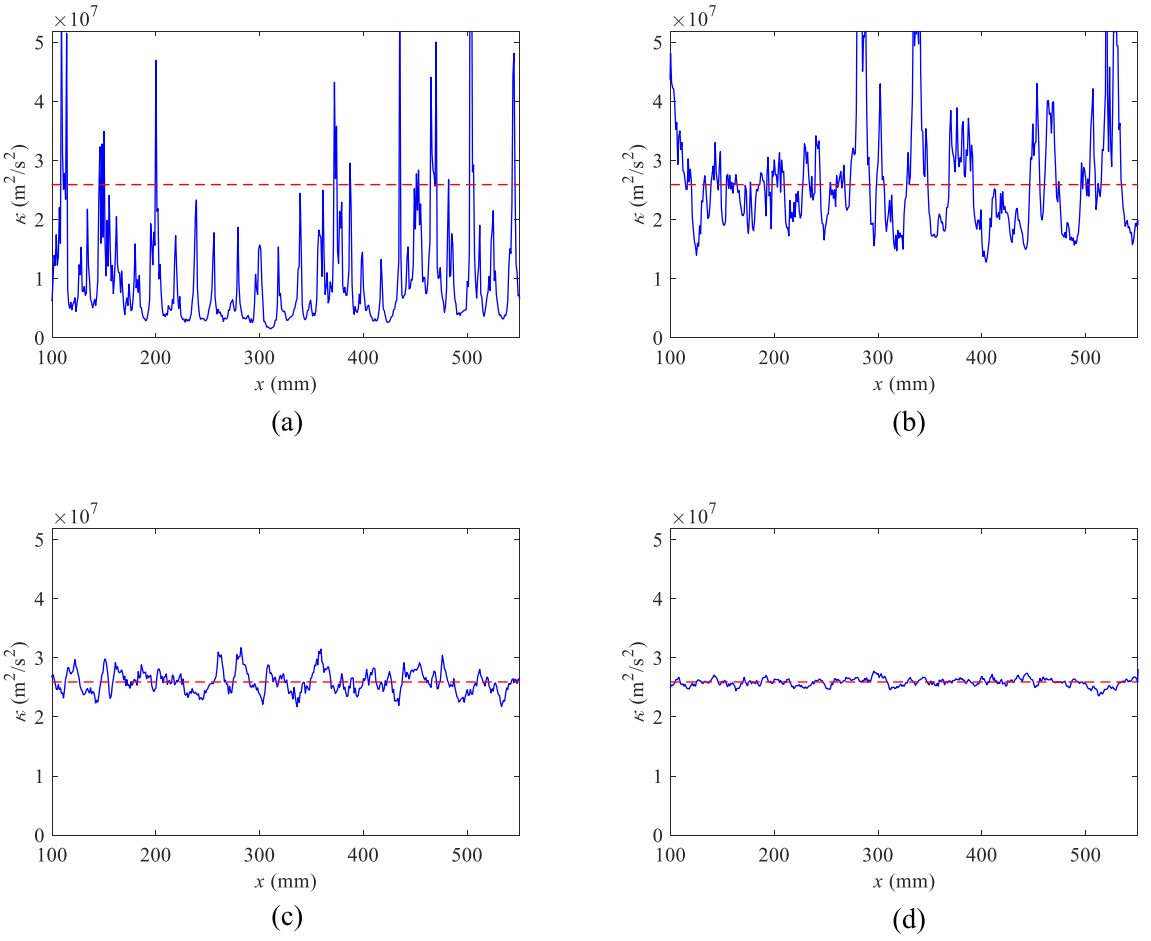

Fig. 12. Enhanced "weak" formulation-based identification results using different scale factors with the noisy displacement: (a) τ = 40 mm, (b) τ = 60 mm, (c) τ = 80 mm and (d) τ = 100 mm.

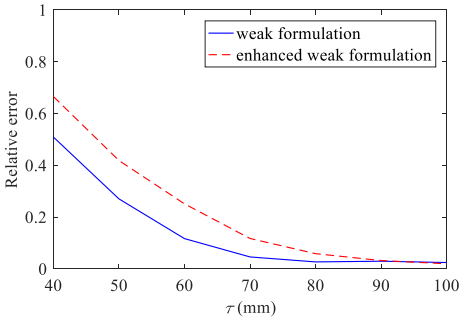

Fig. 13. Relative errors using different values of τ in the "weak" formulation-based methods with the noisy displacement.

to a certain extent when small τ is used. This is different from the conclusion drawn in the absence of the noise shown in Fig. 10. Although, the error near the vibration node can be eliminated because of the use of $w^{(1)}(x)$, the introduction of the 1st order finite difference slightly reduces the noise immunity capability when a small τ is used.

To quantify the noise robustness against different noise levels, the relative error of the enhanced "weak" formulation-based method with different *SNR*s is illustrated in Fig. 14. Obviously, a lower *SNR* would need a larger τ. However, a smaller τ is needed to improve the spatial resolution of the identification. It is therefore crucial to strike a balance between the noise immunity capability and the spatial resolution for the enhanced "weak" formulation-based method.

4. Numerical study on the stiffness changes due to the thickness reduction

To further validate the effectiveness of the proposed method in identifying the local specific stiffness of a structure, a step-shaped beam, made of aluminum, is considered. Detailed geometrical parameters are shown in Fig. 15. The beam thickness is 5 mm at the left end, reduced by 0.5 mm and 1 mm sequentially. A harmonic point-excitation force is applied at x = 1000 mm at 200 Hz. Again, a finite element model is created using beam element of 1 mm long. ABAQUS is used and a Gaussian white noise with a standard deviation of 1‰ in the magnitude is then added to create the noisy vibration displacement data set.

Using the vibration displacement without and with the added noise, the constructed local specific stiffness curves using the enhanced "weak" formulation-based method are shown in Figs. 16 and 17, respectively. Assuming that the thickness reduction is unknown, an equivalent drop in the local specific stiffness can be detected using the proposed method. Considering a beam with a rectangular cross-section in this case, the cross-sectional moment of inertia I and cross sectional area S can be written as

$$I = \frac{bh^3}{12} \tag{15}$$

$$S = hb \tag{16}$$

where h and b are the thickness and the width of the beam structure. According to Eq. (3), the specific stiffness κ and the thickness h satisfy

$$\kappa h^2 = \frac{12\omega^2 w(x)}{w^{(4)}(x)} \tag{17}$$

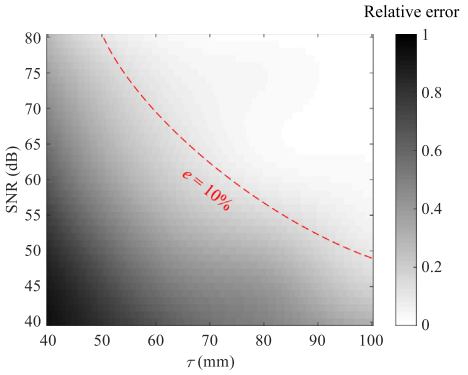

Fig. 14. Relative error under different noise levels using the enhanced "weak" formulation-based method.

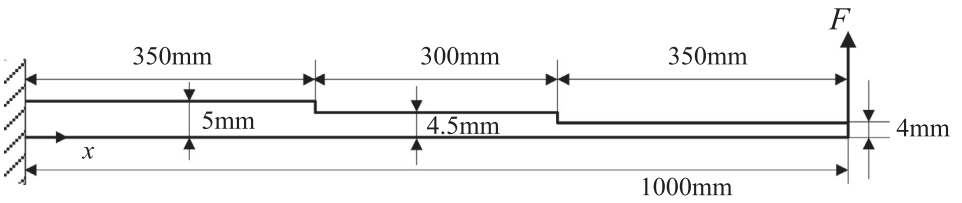

Fig. 15. A step-shaped beam for thickness reduction validation.

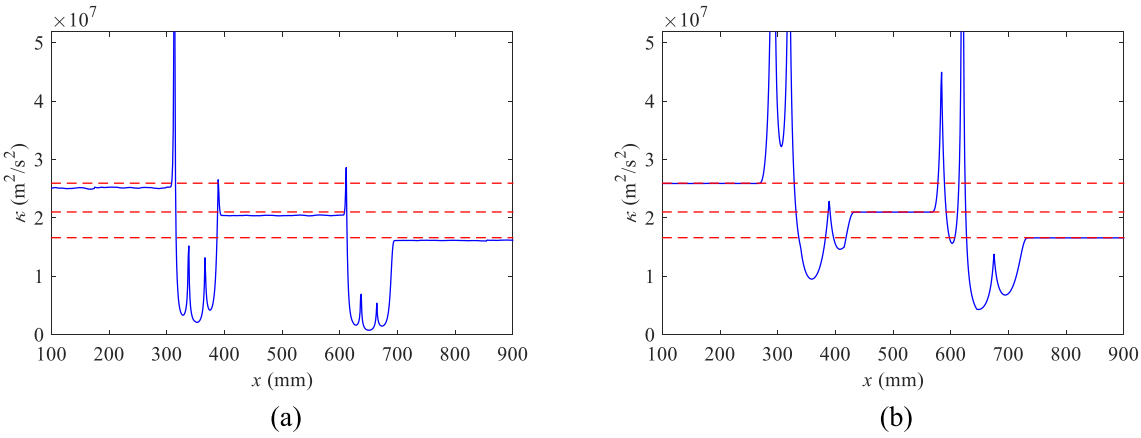

Fig. 16. Thickness reduction detection using the enhanced "weak" formulation-based local stiffness identification with different τ: (a) τ = 40 and (b) 80 mm.

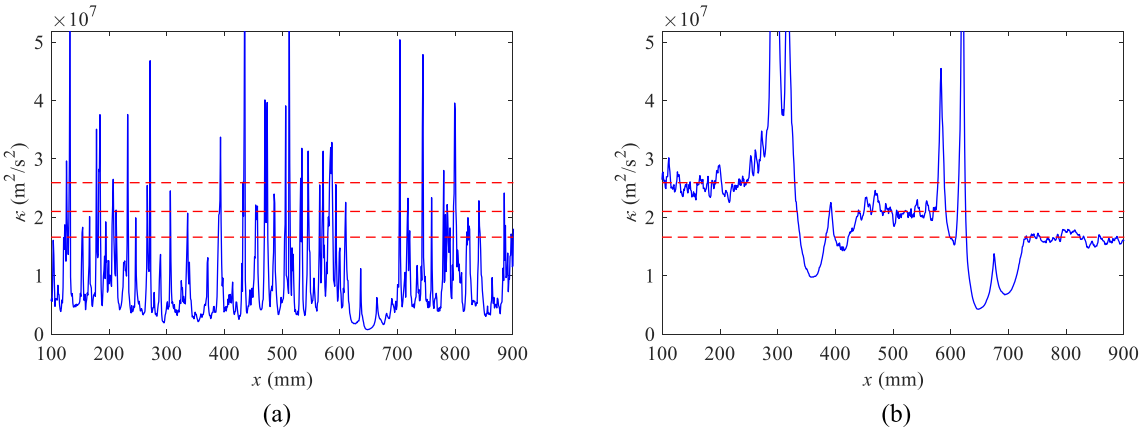

Fig. 17. Thickness reduction detection under noisy condition using the enhanced "weak" formulation-based local stiffness identification with different τ: (a) τ = 40 and (b) 80 mm.

Therefore, the equivalent drop in the local specific stiffness would be equal to the reduction in the square of the thickness, which can be calculated as marked in the dotted line in Figs. 16 and 17.

As representative results in Fig. 16, the enhanced "weak" formulation-based method can identify the local thickness of the beam clearly with different τ, showing the stepped shape along the beam length. However, when a Gaussian white noise is added, only when τ = 80 can obtain a satisfactory detection. As anticipated, increasing the scale factor τ is an effective way to improve the noise immunity capability of the proposed method.

It is pertinent to note that the abrupt change in the thickness (at x = 350 and 650 mm) affects the identified $\widetilde{\kappa}$ curve significantly. When the step is involved in the weight function, the assumption that the parameters (E and I) are constants in the space domain cannot be satisfied. Meanwhile, the discontinuity in the vibration displacement and its fourth order derivative is inevitably greatly magnified. Reaching these locations, the discontinuous effect will be extended to the vicinity of the step when a scanning window is used in the enhanced "weak" formulation-based method, affecting the nearby areas as observed in Figs. 16 and 17. Therefore, the selection of the scale factor τ plays a vital role in balancing the noise immunity capability and the length of the disrupted area.

5. Experimental validations

5.1. Setup

Experimental validations are subsequently carried out using the same step-shaped beam involving thickness reductions. The aluminum structure, with dimensions depicted in Fig. 18, is fix-supported at the left end and excited by an electromechanical shaker at x = 990 mm, producing a harmonic point-force excitation at 200 Hz (referring to the coordinate system in

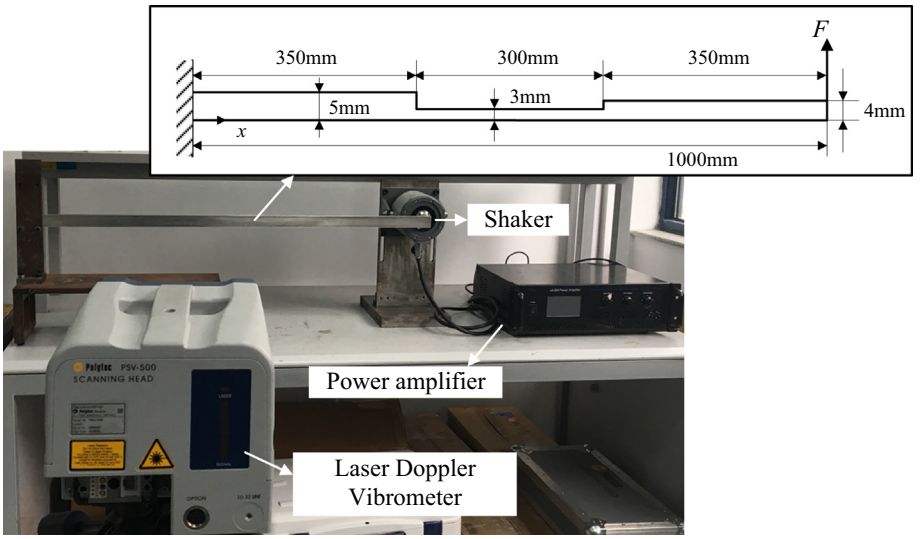

Fig. 18. Experimental setup and structural dimensions.

Fig. 18 and the coordinate origin is located at the left end of the structure). A scanning Laser Doppler Vibrometer (Polytec PSV-500) is used to measure the flexural displacement within the selected inspection region from x = 150 mm to 850 mm on the flat surface without steps. The measurement interval between two adjacent points is 2.74 mm.

5.2. Results and discussions

Considering that the spatial resolution of the equipment in vibration measurement is limited, the interval between two adjacent measurement points is much larger than that in the numerical simulation. Therefore, in order to keep a high sampling accuracy in the weight function and the inner product operation, the vibration displacement measured by the PSV-500 is resampled using shape-preserving piecewise cubic interpolation. The original measurement interval is divided into three segments, thus increasing the spatial resolution from 2.74 mm to 0.91 mm. The resampled vibration displacement, which is used in the subsequent identification process, is shown in Fig. 19.

The enhanced "weak" formulation-based method is used. The local specific stiffness curves along the beam structure, identified from the measured vibration displacement, are shown in Fig. 20. Four different scale factors with $\tau \leq 100$ mm are used. Two large saltation points can be observed at x = 350 mm and 650 mm, where the thickness of the beam changes in stepped variation. The disturbed areas induced by this discontinuous effect are also extended to the vicinity of the step. Thanks to the high signal-to-noise ratio of the measurement, three steps of the equivalent local specific stiffness can be observed with $\tau \geq 80$ mm. The equivalent $\widetilde{\kappa}$ are 2.59×10^7 m^2/s^2, 0.93×10^7 m^2/s^2 and 1.66×10^7 m^2/s^2, corresponding to the thickness of 5 mm, 3 mm and 4 mm, respectively. Consistent with the preceding theoretical and numerical analyses, the downwards trend of the noise induced oscillation in $\widetilde{\kappa}$ curves can be observed by increasing the scale factor of the weight function. From Fig. 20(a) to (d), the outline of the stepped beam becomes more and more apparent, showing the validity and the accuracy of the proposed method in local specific stiffness identification.

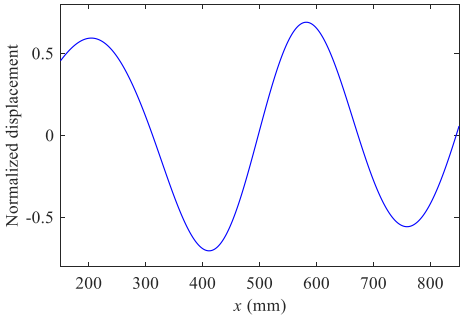

Fig. 19. Normalized vibration displacement at 200 Hz used in the experimental validation.

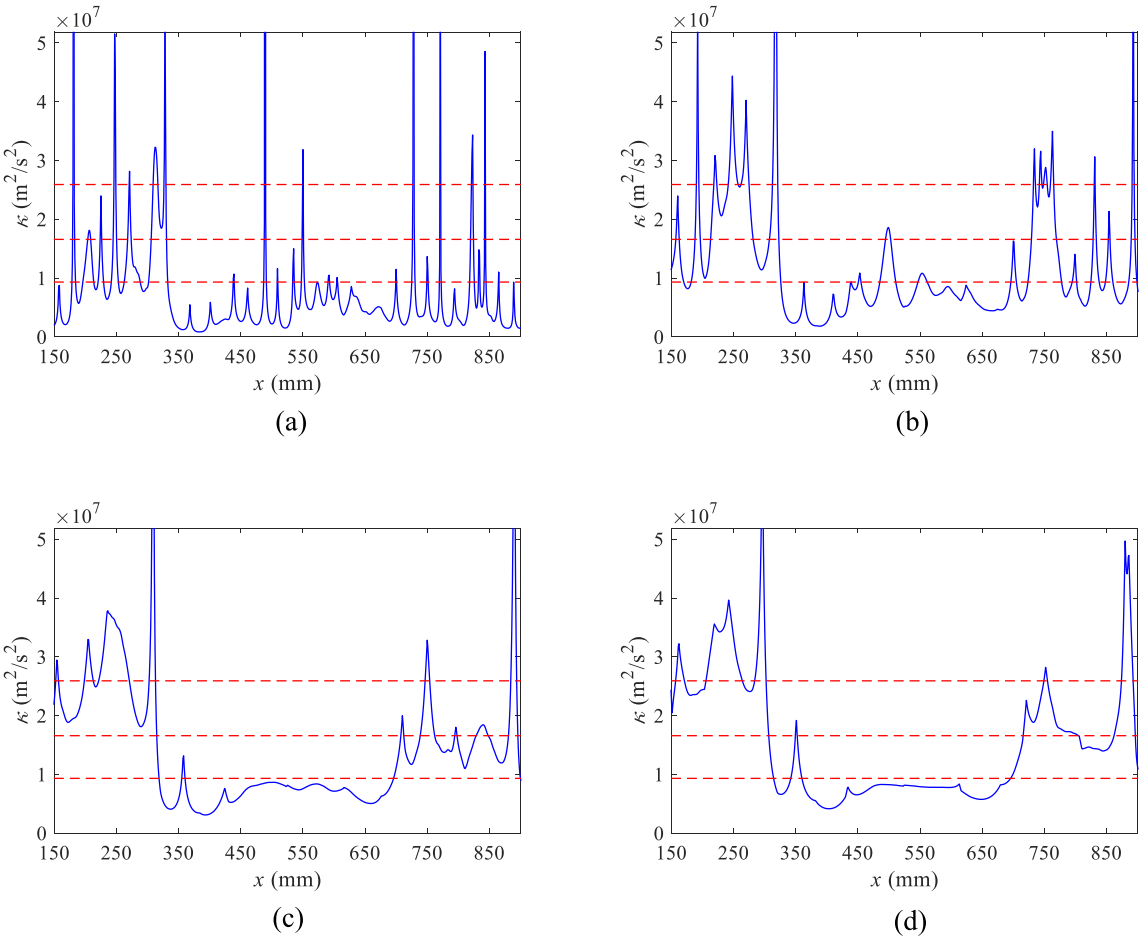

Fig. 20. Experimental results using the enhanced "weak" formulation-based thickness reduction detection with different scale factors: (a) τ = 40, (b) 60, (c) 80 and (d) 100 mm.

It can be seen from Eqs. (1) to (11) that the requirement for the proposed method is to obtain the steady vibration displacement. The material parameter κ, in principle, can be identified under any excitation frequency. In the case that the excitation is not harmonic, the vibration displacement at one frequency component in the frequency domain can also be used after Fourier transform. Therefore, by using a broadband excitation signal, such as a periodic chirp signal [21], the proposed

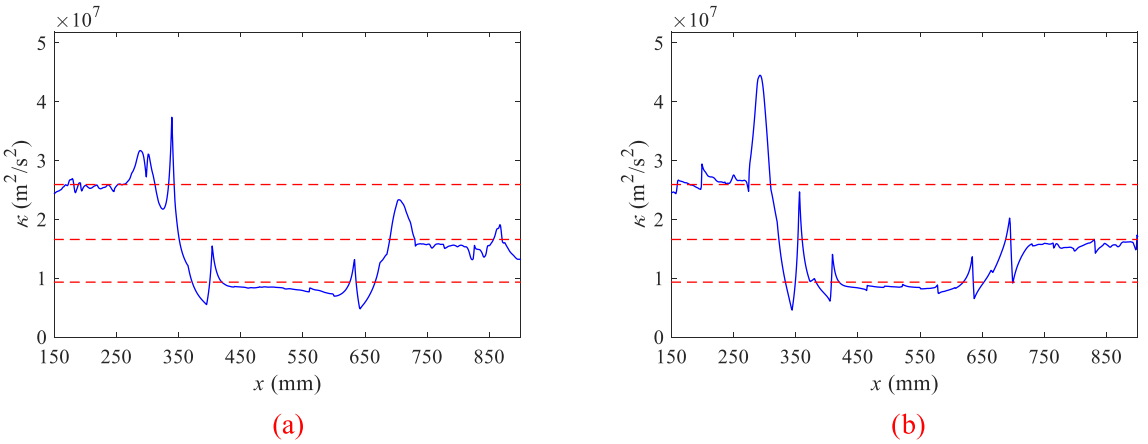

Fig. 21. Experimental results using the enhanced "weak" formulation-based thickness reduction detection with τ = 80 mm when the excitation frequency is (a) 1 kHz and (b) 2 kHz.

method can even trace κ according to frequency. The selection of 200 Hz in both numerical and experimental validations is just an example to show the validity of the proposed method without loss of generality. In order to evaluate the potential of the proposed method in practical applications when the excitation frequency cannot be selected arbitrarily, the experiments using the excitations with 1 kHz and 2 kHz are carried out. The identified $\widetilde{\kappa}$ curves using the enhanced "weak" formulation with τ = 80 mm are illustrated in Fig. 21. The changes in local specific stiffness show the outline of the stepped beam, whilst showing the feasibility of the proposed method for other frequencies.

6. Conclusions

An enhanced multi-scale "weak" formulation is developed in this paper to identify the local specific stiffness of a structure, exemplified by a benchmark beam structure. Compared with the original Pseudo-Excitation approach, the proposed method can not only detect the discontinuous changes induced by structural damage, but also quantitatively identify the equivalent local specific stiffness. To tackle the inherent noise immunity problem in the "strong" formulation-based method, a power-of-cosine weight function is employed as a smooth region scanner, instead of a point detector. In this way, the estimation of the high order derivative through finite difference calculation, required by the strong formulation-based method, is avoided. The robustness of the proposed method is investigated using Gaussian white noise with different *SNR*s. The influences of several key parameters, involved in both the "strong" and "weak" formulation-based methods, are investigated, such as measurement interval, scale factor and the derivative order. Taking a step-shaped beam structure as an example, both numerical analyses and experimental validations are carried out. Variations in the beam thickness can be detected and depicted through the identified $\widetilde{\kappa}$ curves. Results show the significant improvement of the proposed method, as compared with the original strong version, in terms of noise immunity and identification accuracy.

CRediT authorship contribution statement

Chao Zhang: Conceptualization, Writing - original draft. **Hongli Ji:** Investigation, Validation. **Jinhao Qiu:** Methodology, Project administration. **Li Cheng:** Conceptualization, Resources. **Weixing Yao:** Resources. **Yipeng Wu:** Formal analysis.

Declaration of Competing Interest

The authors declare that they have no known competing financial interests or personal relationships that could have appeared to influence the work reported in this paper.

Acknowledgments

This work was supported by National Natural Science Foundation of China (51805261 & 51875277), Natural Science Foundation of Jiangsu Province (BK20180430), China Postdoctoral Science Foundation funded project (2017M621741), Jiangsu Planned Projects for Postdoctoral Research Funds (1701103C), Aeronautical Science Fund (20170252005), Fundamental Research Funds for the Central Universities (NS2018008) and State Key Laboratory of Mechanics and Control of Mechanical Structures (MCMS-I-0518K01 & MCMS-I-0519G02 & MCMS-E-0520K01).

References

[1] S. Das, P. Saha, S. Patro, Vibration-based damage detection techniques used for health monitoring of structures: a review, J. Civil Struct. Health Monitor. 6 (2016) 477–507.
[2] B. Shi, P. Qiao, A new surface fractal dimension for displacement mode shape-based damage identification of plate-type structures, Mech. Syst. Sig. Process. 103 (2018) 139–161.
[3] M. Cao, W. Ostachowicz, R. Bai, M. Radzienski, Fractal mechanism for characterizing singularity of mode shape for damage detection, Appl. Phys. Lett. 103 (2013) 101910–1101451.
[4] A. Pau, A. Greco, F. Vestroni, Numerical and experimental detection of concentrated damage in a parabolic arch by measured frequency variations, J. Vib. Control 17 (2011) 605–614.
[5] P. Nandakumar, K. Shankar, Multiple crack damage detection of structures using the two crack transfer matrix, Struct. Health Monitor. 13 (2014) 548–561.
[6] F. Zahedi, H. Huang, Time–frequency analysis of electro-mechanical impedance (EMI) signature for physics-based damage detections using piezoelectric wafer active sensor (PWAS), Smart Mater. Struct. 26 (2017) 055010.
[7] J. Ciambella, F. Vestroni, The use of modal curvatures for damage localization in beam-type structures, J. Sound Vib. 340 (2015) 126–137.
[8] M. Cao, W. Ostachowicz, M. Radzienski, W. Xu, Multiscale shear-strain gradient for detecting delamination in composite laminates, Appl. Phys. Lett. 103 (2013) 254101.
[9] W. Xu, M. Radzieński, W. Ostachowicz, M. Cao, Damage detection in plates using two-dimensional directional Gaussian wavelets and laser scanned operating deflection shapes, Struct. Health Monitor. 12 (2013) 457–468.
[10] C. Zhang, L. Cheng, J. Qiu, H. Wang, Damage detection based on sparse virtual element boundary measurement using metal-core piezoelectric fiber, Struct. Health Monitor. 17 (2018) 15–23.
[11] L. Campeiro, R. Silveira, F. Baptista, Impedance-based damage detection under noise and vibration effects, Struct. Health Monitor. 17 (2018) 654–667.
[12] F. Santos, B. Peeters, J. Lau, W. Desmet, L. Goes, The use of strain gauges in vibration-based damage detection, J. Phys. Conf. Ser. 628 (2015) 012119.
[13] H. Xu, Z. Su, L. Cheng, J. Guyader, On a hybrid use of structural vibration signatures for damage identification: a virtual vibration deflection (VVD) method, J. Vib. Control 23 (2017) 615–631.

[14] H. Xu, L. Cheng, Z. Su, J. Guyader, Identification of structural damage based on locally perturbed dynamic equilibrium with an application to beam component, J. Sound Vib. 330 (2011) 5963–5981.
[15] H. Xu, Z. Su, L. Cheng, J. Guyader, A "Pseudo-excitation" approach for structural damage identification: from "Strong" to "Weak" modality, J. Sound Vib. 337 (2015) 181–198.
[16] C. Pezerat, J. Guyader, Identification of vibration sources, Appl. Acoust. 61 (2000) 309–324.
[17] S. Chesne, C. Pezerat, J. Guyader, Identification of plate boundary forces from measured displacements, J. Vib. Acoust. 130 (2008) 041006.
[18] H. Xu, L. Cheng, Z. Su, J. Guyader, Damage visualization based on local dynamic perturbation: theory and application to characterization of multi-damage in a plane structure, J. Sound Vib. 332 (2013) 3438–3462.
[19] H. Xu, Z. Su, L. Cheng, J. Guyader, P. Hamelin, Reconstructing interfacial force distribution for identification of multi-debonding in steel-reinforced concrete structures using noncontact laser vibrometry, Struct. Health Monitor. 12 (2013) 507–521.
[20] C. Zhang, L. Cheng, J. Qiu, H. Ji, J. Ji, Structural damage detections based on a general vibration model identification approach, Mech. Syst. Sig. Process. 123 (2019) 316–332.
[21] F. Ablitzer, C. Pézerat, J. Génevaux, J. Bégué, Identification of stiffness and damping properties of plates by using the local equation of motion, J. Sound Vib. 333 (2014) 2454–2468.
[22] F. Wu, W. Yao, A fatigue damage model of composite materials, Int. J. Fatigue 32 (2010) 134–138.
[23] C. Tao, H. Ji, J. Qiu, C. Zhang, Z. Wang, W. Yao, Characterization of fatigue damages in composite laminates using Lamb wave velocity and prediction of residual life, Compos. Struct. 166 (2017) 219–228.
[24] J. Zhao, J. Qiu, H. Ji, Reconstruction of the nine stiffness coefficients of composites using a laser generation based imaging method, Compos. Sci. Technol. 126 (2016) 27–34.
[25] J. Vishnuvardhan, C. Krishnamurthy, K. Balasubramaniam, Genetic algorithm reconstruction of orthotropic composite plate elastic constants from a single non-symmetric plane ultrasonic velocity data, Compos. B Eng. 38 (2007) 216–227.
[26] S. Hwang, J. Wu, R. He, Identification of effective elastic constants of composite plates based on a hybrid genetic algorithm, Compos. Struct. 90 (2009) 217–224.
[27] L. Nan, M. Tahar, Z. Aboura, K. Khellil, A dynamic analysis approach for identifying the elastic properties of unstitched and stitched composite plates, Compos. Struct. 152 (2016) 959–968.
[28] Q. Leclère, F. Ablitzer, C. Pézerat, Practical implementation of the corrected force analysis technique to identify the structural parameter and load distributions, J. Sound Vib. 351 (2015) 106–118.
[29] B. Lascoup, F. Ablitzer, C. Pézerat, Broadband identification of material properties of an orthotropic composite plate using the force analysis technique, Exp. Mech. 58 (2018) 1339–1350.
[30] C. Zhang, L. Cheng, H. Xu, J. Qiu, Structural damage detection based on virtual element boundary measurement, J. Sound Vib. 372 (2016) 133–146.
[31] Q. Leclere, C. Pézerat, Vibration source identification using corrected finite difference schemes, J. Sound Vib. 331 (2012) 1366–1377.